Super-resolved pure-transverse focal fields with an enhanced energy density by focusing an azimuthally polarized first-order vortex beam

Xiangping Li[1], Priyamvada Venugopalan[1], Haoran Ren[1], Minghui Hong[2] and Min Gu[1,*]

[1]*Centre for Micro-Photonics, Faculty of Science, Engineering and Technology, Swinburne University of Technology, Hawthorn, Victoria 3122, Australia*
[2]*Deptartment of Electrical and Computer Engineering, National University of Singapore, Singapore*
**Corresponding author: mgu@swin.edu.au*

Received Month X, XXXX; revised Month X, XXXX; accepted Month X, XXXX; posted Month X, XXXX (Doc. ID XXXXX); published Month X, XXXX

We report on the experimental demonstration of super-resolved pure-transverse focal fields through focusing an azimuthally polarized first-order vortex beam. The optimized confinement of focal fields by creating the constructive interference through the superposition of the first-order vortex on an azimuthally polarized beam is observed by both a scanning near-field microscope and a two-photon fluorescence microscope. An enhanced peak intensity of the focal spot by a factor of 1.8 has been observed compared with that of the unmodulated azimuthally polarized beam. The super-resolved and pure-transverse focal fields with a 31% reduced focal area determined by the full width at half maximum compared to that of tightly focused circular polarization is experimentally corroborated. This superiority over the circular polarization stands for any numerical aperture greater than 0.4. This technique holds the potential for applications requiring sub-wavelength resolution and pure-transverse fields such as high-density optical data storage and high-resolution microscopy.

OCIS Codes: (260.5430) Polarization, (180.1790) Confocal microscopy, (180.4243) Near-field microscopy.

As one of its fundamental aspects, focused light under optical microscopy [1, 2] can selectively interact with anisotropic materials through its polarization state [3], which provides the basic principle of polarization-sensitive nanophotonic devices. In particular, pure-transverse focal fields are highly desired for energy efficient microscopic applications in harmonic generation [4, 5], single molecule detections [6, 7], coherence tomography [8] and multi-dimensional optical data storage [9-12]. In this context, the transversely polarized beam such as the linear and circular polarization focused by an objective lens with a high numerical aperture (NA) is essential for a high microscopic resolution with a high energy density of transverse focal fields. However, the depolarization effect leads to the degraded transverse polarization purity of a linearly and circularly polarized beam with a 17% of energy loss at tightly focusing condition by an objective with a high NA of 1.4 through the emergence of longitudinal field components [13-15].

Owing to its symmetry in a tangential polarization distribution, the azimuthally polarized beam can lead to pure-transverse focal fields disregarding the NA of the objective lens [16, 17]. However, the deconstructive interference between its transverse focal field components can only result in a wide doughnut-shaped focus [18], degrading the energy density of the focal fields [19]. On the other hand, producing super-resolved focal fields through creating constructive interference between its transverse focal field components can significantly enhance the focal energy density. Therefore, generating sharper focal fields of modulated azimuthally polarized beams becomes a subject received numerous theoretical investigations [20-22].

In this letter, we present the experimental demonstration of the super-resolved pure-transverse focal fields through focusing an azimuthally polarized beam superimposed with the first-order vortex (FOV) phase. An enhanced peak intensity of the focal spot by a factor of 1.8 has been observed compared to that of the unmodulated azimuthally polarized beam. The pure-transverse focal field with a 31% of reduced full width at half maximum (FWHM) can be achieved at tightly focused condition at NA=1.4 compared with that of a circularly polarized beam. Moreover, the superiority over the circular polarization maintains even at moderate focusing conditions.

The scheme of creating constructive interference between the transverse focal field components through superimposing the FOV phase is illustrated in Fig.1(a). The focal fields of such an azimuthally polarized FOV beam can be given as,

$$\boldsymbol{E}(r,\varphi,z) = \frac{\pi}{\lambda}(\boldsymbol{E_x} - i\boldsymbol{E_y}) \qquad (1)$$

$$\boldsymbol{E_x} = \int_0^{\alpha} P(\theta)\sin\theta\{-\exp[i2\varphi]J_2(krsin\theta) - J_0(krsin\theta)\} \exp(-ikzcos\theta)d\theta \qquad (2)$$

$$\boldsymbol{E_y} = \int_0^{\alpha} P(\theta)\sin\theta\{-\exp[i2\varphi]J_2(krsin\theta) + J_0(krsin\theta)\} \exp(-ikzcos\theta)d\theta \qquad (3)$$

where $P(\theta)$ is the sine condition of the apodization function and α is the convergence angle given by the NA. Fig. 1(a) shows the numerical calculation of the focal fields by an objective with a high NA=1.4 following the Eqs. (1) to (3). Indeed, the FOV phase can create constructive interference and gain the analogous advantage of the radial polarization, resulting in a tight confinement described by the zero-order Bessel function accompanied by a negligible side lobe with a second-order Bessel distribution. The longitudinal component is null due to the axial depolarization-free nature associated with the tangential polarization distribution of such a modulated azimuthally polarized beam.

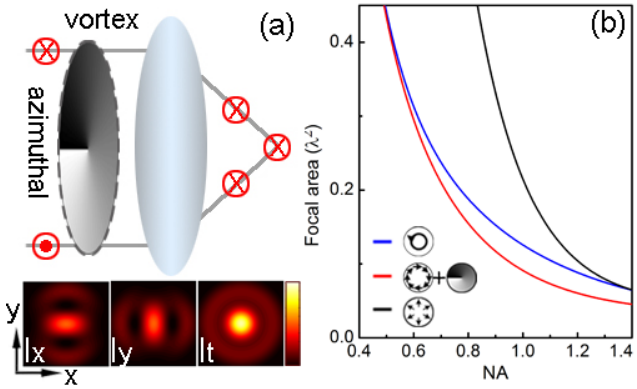

Fig. 1. (color online) (a) Schematic illustration of creating the constructive interference between the transverse focal field components through the superposition of the FOV phase. Intensity patterns of focal fields of an azimuthally polarized beam superimposed the FOV phase. NA=1.4 was used in the calculation. The image size is 1 μm. (b) The numerical comparison of focal areas of an azimuthally polarized FOV beam (red curve), a circularly polarized beam (blue curve) and a radially polarized beam (black curve) as a function of NA.

Fig. 1(b) shows that this superiority in the focal areas maintains even at moderate focusing conditions. The focal area is defined by its FWHM as $A = \pi/4 * f_x * f_y$, where $f_{x/y}$ is the FWHM at the x- and y-directions. The focal area of the azimuthally polarized FOV beam is notably smaller than that of the circularly polarized beam once the NA of the objective is greater than 0.4. This can be attributed to the fact that the FOV modulated azimuthally polarized beam with opposite sides of the pupil being in phase can lead to a tightly focused in-plane electric field components. In addition, the depolarization-free nature results in a null of the longitudinal field components, which have a doughnut-shaped distribution and are responsible for widening the distribution of the focal spot for a circularly polarized beam. However, it is far better than that of a radially polarized beam, which has been intensively studied for a sharper focus at tightly focused condition [23-25], ranging from a small NA to a high NA of 1.4. At the high NA of 1.4, the obtained focus has a significantly smaller focal area ($0.089\lambda^2$ for single-photon excitation and $0.045\lambda^2$ for two-photon excitation), corresponding to 31% and 28% smaller than that of a circularly and radially polarized beam, respectively.

To verify the optimized confinement of pure-transverse focal fields, the spatial distribution of its focal fields of an azimuthally polarized beam superimposed with the FOV phase was mapped through scanning near-field microscopy (SNOM). The experimental configuration is illustrated in Fig. 2(a). To keep the generality, an objective with a low NA of 0.7 was employed to focus the modulated azimuthal beam. In order to accurately map the transverse focal fields, an elliptical-shaped SNOM tip (inset of Fig. 2(a)) with an in-plane polarization sensitivity was employed [26, 27]. It has a linear polarization sensitivity along its short axis [26]. Figs. 2(b) to (c) show the intensity distributions of the focal fields of a tightly focused azimuthally polarized beam with the polarization-sensitive axis of the SNOM tip along the x- and y-directions, respectively. A doughnut-shaped distribution with a hollow intensity at its center can be clearly evident [17, 18]. In addition, the peak intensity of the solid focal spot was measured to be approximately 1.8 times stronger than that of the doughnut-shaped wide focus, which is consistent with the calculation.

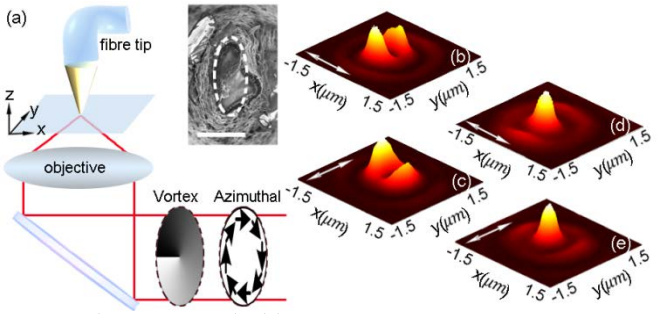

Fig. 2. (color online) (a), Experimental configuration of near-field mapping of focal fields of a modulated azimuthally polarized beam. (b) and (c) The normalized intensity distribution of E_x and E_y components of an azimuthally polarized beam, respectively. (d) and (e) The normalized intensity distribution of E_x and E_y components of an azimuthally polarized beam superimposed with the FOV phase, respectively.

In the presence of the FOV phase, the hollow intensity at the center of the focal area is removed. The FOV phase modulation generates a solid focal spot with a remarkably smaller distribution. A tight lateral confinement in the y-direction for E_x with a FWHM of 0.52λ at a moderate focusing condition by an objective with NA=0.7 can be clearly revealed, as shown in Figs. 2(d). Although this advantage is obtained at the cost of an increased side lobes, the intensities are negligible with less than 15% of the main peak. By rotating the polarization-sensitive axis of the SNOM tip 90 degrees, a similar confinement in the

x-direction for E_y can be found in Fig. 2(e). This feature is consistent with the calculations following Eqs. (1) to (3) as depicted in Fig. 1(a).

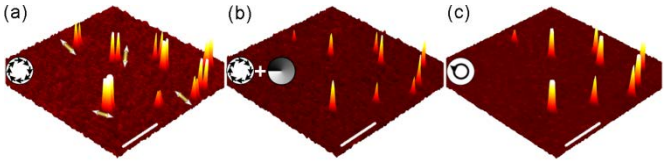

Fig. 3. (color online) TPF imaging of single gold nanorods by an azimuthally polarized beam (a), an azimuthally polarized beam superimposed with the FOV phase (b), and a circularly polarized beam (c). The white double arrows schematically illustrate the orientation of the selected gold nanorods. The scale bars are 6 μm. To keep a clear signal-noise-ratio in the TPF image, the intensities of the azimuthally and circularly polarized beams were kept double of that of the azimuthally polarized FOV beam.

Besides a tight spatial confinement, the FOV can produce a $\frac{\pi}{2}$-phase retardation between the E_x and E_y component, and convert the azimuthal polarization to the quasi-circular polarization state on the focal axis, as depicted in Eqs. (1) to (3). This feature was also experimentally corroborated by the two-photon fluorescence (TPF) imaging of single gold nanorods, which were widely used to verify the focal polarization states through the sharp polarization photoresponse [7, 28, 29]. Gold nanorods with random in-plane orientations can be clearly distinguished from their characteristic two-lobe TPF intensity patterns when illuminated by the azimuthally polarized beam, as shown in Fig. 3(a). A few rods with different orientations indicated by the arrows are chosen as an example. Fig. 3(b) shows that gold nanorods with different orientations can be simultaneously excited by the azimuthally polarized beam superimposed with the FOV phase and the two-lobe intensity patterns were changed to solid spots. For comparison, the TPF image of the same gold nanorods obtained by a circularly polarized beam is also shown in Fig. 3(c) with identical intensity patterns. This result implies that the focal polarization state of the modulated azimuthally polarized beam is indeed converted to that of a quasi-circularly polarized beam in the focal region.

Fig. 4(a) depicts the comparison of the cross section plots between point spread functions (PSFs) obtained in the TPF imaging of a single gold nanorod by a circularly polarized beam and an FOV-phase modulated azimuthally polarized beam through an objective with a high NA=1.4. To this purpose, gold nanorods with a size of 15 nm by 40 nm were prepared and sparsely distributed on a cover glass. The measured FWHM of the PSF of the FOV-phase modulated azimuthally polarized beam (0.25λ) is remarkably smaller than that of the circularly polarized beam (0.3λ). In addition, the calculated optical transfer functions (OTFs) of such a circularly and FOV modulated azimuthally polarized beam, obtained through the Fourier transfer of their point spread functions given by an objective with high NA of 1.4, are shown in the insets of Fig. 4(a). Indeed, extended spatial frequencies for the azimuthally polarized FOV beam beyond the cutoff of the circularly polarized beam (indicated by the dashed circles) can be clearly verified.

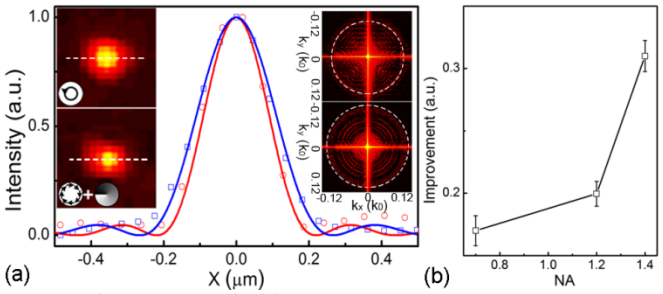

Fig. 4. (color online) (a) Cross section plots of the TPF PSFs by a circularly polarized beam (blue squares) and an azimuthally polarized beam superimposed with the FOV phase (red circles) under an objective with high NA =1.4. The solid lines represent the fittings. The insets in the left panel show the TPF image of a single gold nanorod by a circularly polarized beam and an azimuthally polarized beam superimposed the FOV phase. The dashed lines indicate the cross sections. The insets in the right panel show the OTFs for the normalized spatial frequencies of the circularly and FOV modulated azimuthally polarized beam, respectively. The dashed circles indicate the cutoff of spatial frequencies supported. $k_0 = 2\pi/\lambda$. (b) Improvement of the focal area of an azimuthally polarized beam FOV beam compared with that of a circularly polarized beam at different values of NA.

The improvement in the super-resolved focal area is experimentally corroborated at focusing conditions with NA ranged from 0.7 to 1.4, as shown in Fig. 4(b). At the tightly focused condition by NA=1.4, the measured focal area of the FOV-phase modulated azimuthally polarized beam is approximately $0.049\lambda^2$, corresponding to a 31% reduction compared to the circularly polarized beam. This improvement decreases to 17% as the NA reduces to 0.7. It should be noted that a further improvement of the lateral resolution is possible by applying apodization methods on the modulated azimuthal beam [21].

In conclusion, we have demonstrated the super-resolved pure-transverse focal fields with an enhanced focal energy density through focusing an azimuthally polarized FOV beam. This feature has been achieved through breaking the rotational symmetry in phase of an azimuthally polarized beam to create constructive interference between its transverse focal field components, and experimentally corroborated by both the

near-field mapping and the TPF imaging. The remarkably reduced focal area maintains from the moderate to tight focusing conditions, paving the way for a variety high-resolution microscopic applications.

Acknowledgements: The authors thank the Australian Research Council for its funding support through Laureate Fellowship scheme (FL100100099) and Discovery project (DP110101422).

References

1. W. Denk, J. H Strickler, and W. W. Webb, Science **248**, 73 (1990).
2. J. Bewersdorf, R. Pick, and S. W. Hell, Opt. Lett. **23**, 655-657 (1998).
3. R. M. A. Azzam, and N. M. Bashara, *Ellipsometry and Polarized Light* (North-Holland, 1977).
4. Y. Sheng, S. M. Saltiel, N. Voloch-Bloch, D. N. Neshev, W. Krolikowski, A. Arie, K. Koynov, and Y. S. Kivshar, IEEE J. Quant. Electron. **45**, 1465-1472 (2009).
5. P. Stoller, B. M. Kim, A. M. Rubenchik, K. M. Reiser, and L. B. Da Silva, J. Biomed. Opt. **7**, 205-214 (2002).
6. M. Noto, D. Keng, I. Teraoka, and S. Arnold, Biophys. J. **92**, 4466-4472 (2007).
7. W. S. Chang, J. W. Ha, L. S. Slaughter, and S. Link, Proc. Natl. Acad. Sci. **107**, 2781-2786 (2010).
8. J. F. De Boer, and T. E. Milner, J. Biomed. Opt. **7**, 359-371 (2002).
9. M. Gu, X. Li, and Y. Cao, Light Sci. and Appl. **3**, e177 (2014).
10. P. Zijlstra, J. W. M. Chon, and M. Gu, Nature **459**, 410-413 (2009).
11. X. Li, J. W. M. Chon, S. Wu, R. A. Evans, and M. Gu, Opt. Lett. **32**, 277-279 (2007).
12. X. Li, J. W. M. Chon, R. A. Evans, and M. Gu, Opt. Express **17**, 2954-2961 (2009).
13. M. Gu, *Advanced optical imaging theory* (Springer, 2000).
14. B. Richards, and E. Wolf, Proc. R. Soc. A **253**, 358-379 (1959).
15. X. Li, T. H. Lan, C. H. Tien, and M. Gu, Nat. Commun. **3**, 998 (2012).
16. Q. Zhan, and J. R. Leger, Opt. Express **10**, 324-331 (2002).
17. K. S. Youngworth, and T. G. Brown, Opt. Express **7**, 77-87 (2000).
18. M. Gu, H. Kang, and X. Li, Sci. Rep. **4**, 3627 (2014).
19. M. Gu, H. Lin, and X. Li, Opt. Lett. **38**, 3627-3630 (2013).
20. Y. Jiang, X. Li, and M. Gu, Opt. Lett. **38**, 2957-2960 (2013).
21. X. A. Hao, C. F. Kuang, T. T. Wang, and X. Liu, Opt. Lett. **35**, 3928-3930 (2010).
22. S. Wang, X. Li, J. Zhou, and M. Gu, Opt. Lett., accepted (2014).
23. G. M. Lerman, and U. Levy, Opt. Express **16**, 4567-4581 (2008).
24. R. Dorn, S. Quabis, and G. Leuchs, Phys. Rev. Lett. **91**, 2339011-2339014 (2003).
25. X. Li, Y. Cao, and M. Gu, Opt. Lett. **36**, 2510-2512 (2011).
26. P. Venugopalan, Q. Zhang, X. Li, and M. Gu, Opt. Express **21**, 15247-15252 (2013).
27. P. Biagioni, D. Polli, M. Labardi, A. Pucci, G. Ruggeri, G. Cerullo, M. Finazzi, and L. Duò, Appl. Phys. Lett. **87**, 1-3 (2005).
28. T. Ming, L. Zhao, Z. Yang, H. Chen, L. Sun, J. Wang, and C. Yan, Nano Lett. **9**, 3896-3903 (2009).
29. H. Wang, L. Shi, B. Lukyanchuk, C. Sheppard, and C. T. Chong, Nat. Photonics **2**, 501-505 (2008).

References

1. W. Denk, J. H Strickler, and W. W. Webb, "Two-photon laser scanning fluorescence microscopy," Science **248**, 73 (1990).
2. J. Bewersdorf, R. Pick, and S. W. Hell, "Multifocal multiphoton microscopy," Opt. Lett. **23**, 655-657 (1998).
3. R. M. A. Azzam, and N. M. Bashara, *Ellipsometry and Polarized Light* (North-Holland, 1977).
4. Y. Sheng, S. M. Saltiel, N. Voloch-Bloch, D. N. Neshev, W. Krolikowski, A. Arie, K. Koynov, and Y. S. Kivshar, "Cerenkov-type second-harmonic generation in two-dimensional nonlinear photonic structures," IEEE J. Quant. Electron. **45**, 1465-1472 (2009).
5. P. Stoller, B. M. Kim, A. M. Rubenchik, K. M. Reiser, and L. B. Da Silva, "Polarization-dependent optical second-harmonic imaging of a rat-tail tendon," J. Biomed. Opt. **7**, 205-214 (2002).
6. M. Noto, D. Keng, I. Teraoka, and S. Arnold, "Detection of protein orientation on the silica microsphere surface using transverse electric/transverse magnetic whispering gallery modes," Biophys. J. **92**, 4466-4472 (2007).
7. W. S. Chang, J. W. Ha, L. S. Slaughter, and S. Link, "Plasmonic nanorod absorbers as orientation sensors," Proc. Natl. Acad. Sci. **107**, 2781-2786 (2010).
8. J. F. De Boer, and T. E. Milner, "Review of polarization sensitive optical coherence tomography and Stokes vector determination," J. Biomed. Opt. **7**, 359-371 (2002).
9. M. Gu, X. Li, and Y. Cao, "Optical storage arrays: A perspective for future big data storage," Light Sci. and Appl. **3**, e177 (2014).
10. P. Zijlstra, J. W. M. Chon, and M. Gu, "Five-dimensional optical recording mediated by surface plasmons in gold nanorods," Nature **459**, 410-413 (2009).
11. X. Li, J. W. M. Chon, S. Wu, R. A. Evans, and M. Gu, "Rewritable polarization-encoded multilayer data storage in 2,5-dimethyl-4-(p-nitrophenylazo)anisole doped polymer," Opt. Lett. **32**, 277-279 (2007).
12. X. Li, J. W. M. Chon, R. A. Evans, and M. Gu, "Quantum-rod dispersed photopolymers for multi-dimensional photonic applications," Opt. Express **17**, 2954-2961 (2009).
13. M. Gu, *Advanced optical imaging theory* (Springer, 2000).
14. B. Richards, and E. Wolf, "Electromagnetic diffraction in optical systems II structure of the image field in an aplanatic system," Proc. R. Soc. A **253**, 358-379 (1959).
15. X. Li, T. H. Lan, C. H. Tien, and M. Gu, "Three-dimensional orientation-unlimited polarization encryption by a single optically configured vectorial beam," Nat. Commun. **3**, 998 (2012).
16. Q. Zhan, and J. R. Leger, "Focus shaping using cylindrical vector beams," Opt. Express **10**, 324-331 (2002).
17. K. S. Youngworth, and T. G. Brown, "Focusing of high numerical aperture cylindrical-vector beams," Opt. Express **7**, 77-87 (2000).
18. M. Gu, H. Kang, and X. Li, "Breaking the diffraction-limited resolution barrier in fiber-optical two-photon fluorescence endoscopy by an azimuthally-polarized beam," Sci. Rep. **4**, 3627 (2014).
19. M. Gu, H. Lin, and X. Li, "Parallel multiphoton microscopy with cylindrically polarized multifocal arrays," Opt. Lett. **38**, 3627-3630 (2013).
20. Y. Jiang, X. Li, and M. Gu, "Generation of sub-diffraction-limited pure longitudinal magnetization by the inverse Faraday effect through tightly focusing an azimuthally polarized vortex beam," Opt. Lett. **38**, 2957-2960 (2013).
21. X. A. Hao, C. F. Kuang, T. T. Wang, and X. Liu, "Phase encoding for sharper focus of the azimuthally polarized beam," Opt. Lett. **35**, 3928-3930 (2010).
22. S. Wang, X. Li, J. Zhou, and M. Gu, "Ultra-long pure longitudinal magnetization needle induced by annular vortex binary optics " Opt. Lett., accepted (2014).
23. G. M. Lerman, and U. Levy, "Effect of radial polarization and apodization on spot size under tight focusing conditions," Opt. Express **16**, 4567-4581 (2008).
24. R. Dorn, S. Quabis, and G. Leuchs, "Sharper Focus for a Radially Polarized Light Beam," Phys. Rev. Lett. **91**, 2339011-2339014 (2003).
25. X. Li, Y. Cao, and M. Gu, "Superresolution-focal-volume induced 3:0 Tbytes=disk capacity by focusing a radially polarized beam," Opt. Lett. **36**, 2510-2512 (2011).
26. P. Venugopalan, Q. Zhang, X. Li, and M. Gu, "Polarization-sensitive characterization of the propagating plasmonic modes in silver nanowire waveguide on a glass substrate with a scanning near-field optical microscope," Opt. Express **21**, 15247-15252 (2013).
27. P. Biagioni, D. Polli, M. Labardi, A. Pucci, G. Ruggeri, G. Cerullo, M. Finazzi, and L. Duò, "Unexpected polarization behavior at the aperture of hollow-pyramid near-field probes," Appl. Phys. Lett. **87**, 1-3 (2005).
28. T. Ming, L. Zhao, Z. Yang, H. Chen, L. Sun, J. Wang, and C. Yan, "Strong polarization dependence of plasmon-enhanced fluorescence on single gold nanorods," Nano Lett. **9**, 3896-3903 (2009).
29. H. Wang, L. Shi, B. Lukyanchuk, C. Sheppard, and C. T. Chong, "Creation of a needle of longitudinally polarized light in vacuum using binary optics," Nat. Photonics **2**, 501-505 (2008).